Principles of Designing Extra-Large Pore Openings and Cages in Zeolitic Imidazolate Frameworks

Jingjing Yang,[†,◆] Yue-Biao Zhang,[†,○,◆] Qi Liu,[‡,⊥] Christopher A. Trickett,[†] Enrique Gutiérrez-Puebla,[§] M. Ángeles Monge,[§] Hengjiang Cong,[‡] Abdulrahman Aldossary,[†] Hexiang Deng,*[‡,⊥] and Omar M. Yaghi*[†,⊥,#]

[†]Department of Chemistry, University of California, Berkeley, Materials Sciences Division, Lawrence Berkeley National Laboratory, and Kavli Energy NanoSciences Institute, Berkeley, California 94720, United States

[‡]Key Laboratory of Biomedical Polymers—Ministry of Education, College of Chemistry and Molecular Sciences, Wuhan University, Wuhan 430072, China

[⊥]UC Berkeley, Global Science Institute - Wuhan University, the Insitute of Advanced Studies Joint Innovative Center, Wuhan University, Wuhan 430072, China

[§]Instituto de Ciencia de Materiales de Madrid-CSIC, Sor Juana Inés de la Cruz 3, 20849 Madrid, Spain

[#]King Abdulaziz City for Science and Technology, Riyadh 11442, Saudi Arabia

Ⓢ Supporting Information

ABSTRACT: We report three design principles for obtaining extra-large pore openings and cages in the metal−organic analogues of inorganic zeolites, zeolitic imidazolate frameworks (ZIFs). Accordingly, we prepared a series of 15 ZIFs, members of which have the largest pore opening (22.5 Å) and the largest cage size (45.8 Å) known for all porous tetrahedral structures. The key parameter allowing us to access these exceptional ZIFs is what we define as the steric index (δ), which is related to the size and shape of the imidazolate linkers employed in the synthesis. The three principles are based on using multiple linkers with specific range and ratios of δ to control the size of rings and cages from small to large, and therefore are universally applicable to all existing ZIFs. The ZIF with the largest cage size (ZIF-412) shows the best selectivity of porous materials tested toward removal of octane and p-xylene from humid air.

Steric Index

$\delta = V \times l_{max}$
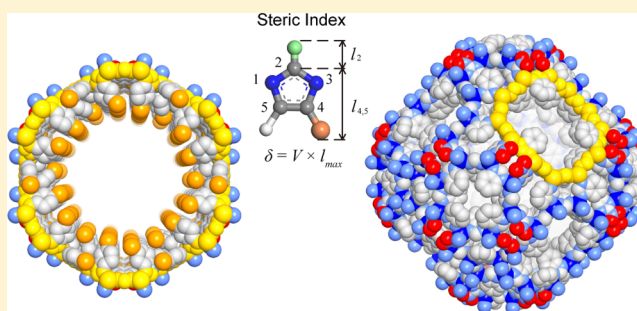
INTRODUCTION

Zeolitic imidazolate frameworks (ZIFs) have emerged as an important class of porous crystals because they are the metal−organic analogues of zeolites: combining tetrahedral extended structures with organic functionality.[1−5] Although guiding principles based on structure directing agents are well-known for zeolites,[6] to date no clear basic principles have emerged for the design of ZIFs.[7−14] Identifying the key parameters in the construction of ZIFs promises to propel the field of porous, crystalline tetrahedral structures into previously unachieved pore size regime and chemistry. Herein, we report 15 ZIFs (ZIF-303, -360, -365, -376, -386, -408, -410, -412, -413, -414, -486, -516, -586, -615, and -725) and three design principles applicable to all known ZIFs: (1) The shape and size of the imidazolate (Im) linker, described by the steric index (δ, Figure 1), determine the maximum possible pore opening. (2) The combination of Im linkers with small and large δ is required for maximum cage size (internal pore) to be achieved. (3) For a given set of Im linkers a diversity of pore metrics can be accessed by varying Im ratios. All these ZIFs were made using different kinds of Im leading to 10 tetrahedral topologies either known in ZIFs but with new composition (CHA, LTA, **moz**, and GME), unrealized in ZIFs (AFX and KFI), or unrealized in any structures (termed **ykh**, **gcc**, **bam**, and **ucb**). Members of this series are ZIFs with permanent porosity that represent the largest pore opening (ZIF-725) and cage size (ZIF-412, 413, and 414) among all tetrahedral porous crystals. We demonstrate that ZIF-412, having the largest cage, can selectively bind large-sized volatile organic compounds, octane and p-xylene. The hydrophobicity and large pore space within this ZIF provide for exceptionally high separation and cycling performance, especially in the presence of water.

EXPERIMENTAL SECTION

General Synthetic Procedure and Characterization of ZIFs. The ZIFs reported in this study were synthesized by mixing two or three Im linkers chosen from among the series IM, nIM, mIM, aIM, 4-nIM, bIM, 2-mbIM, cbIM, mbIM, bbIM, and nbIM (Figure 1) with a zinc(II) salt (nitrate and trifluorosulfate) in N,N-dimethylformamide
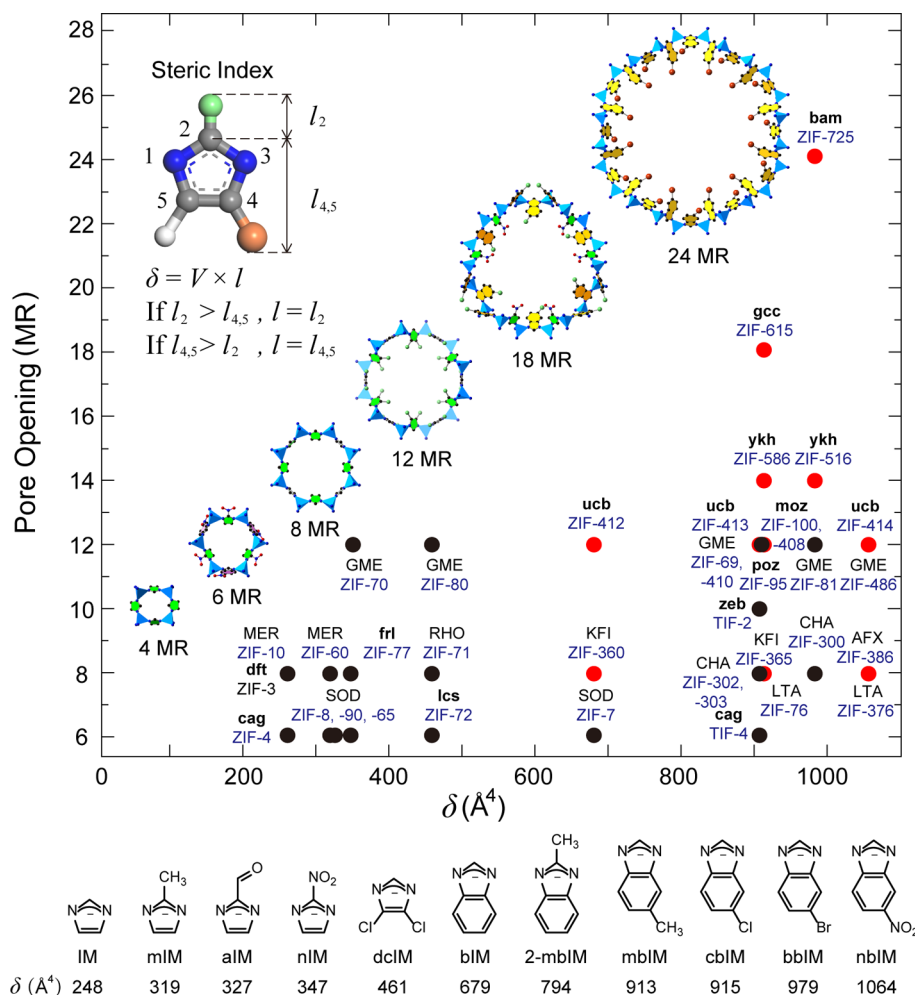
Figure 1. Correlation between the δ values of Im linkers with the largest ring sizes in ZIFs where progressively larger ring sizes (pore opening) are made in ZIFs by increasing Im linkers' size and shape (steric index, δ). The corresponding rings are demonstrated in ball-and-stick images with the ring size shown (N, blue; C, dark; O, red; Cl, green; Br, orange; and ZnN_4 units, light blue tetrahedra. H atoms are omitted for clarity). Several ZIFs made by a bulky solvent templating approach are not plotted (see Table S17 and its note for details). The inset, upper left, shows a schematic of the Im linker including the definition of δ. Molecular structures of Im linkers discussed in this paper are shown along with their respective δ values. Red dots represent structures reported here, and black dots represent those already reported.

or N,N-diethylformamide. Crystals of each of the ZIFs, suitable for single crystal X-ray diffraction analysis, were obtained after heating the solution within the temperature range 65−130 °C and for a period of 3−30 days. Varying the combination and stoichiometry of Im linkers led to the discovery of 15 new ZIFs with their structures identified by using either synchrotron or laboratory based X-ray diffraction techniques. The exact molar ratio of the Im linkers in each ZIF was further confirmed by ^{1}H NMR spectroscopy and elemental microanalyses of the guest-free samples. Detailed procedures and characterizations are provided in Supporting Information (SI)

Topology Analysis. Seven of these new ZIFs have topologies belonging to known zeolites (ZIF-303, CHA; ZIF-360 and -365, KFI; ZIF-376, LTA; ZIF-386, AFX; ZIF-410 and -486, GME, respectively), among which the KFI and AFX topologies were achieved for the first time in ZIFs. The other eight new ZIFs have tetrahedral topologies. Topologies unrealized in zeolites (ZIF-408, **moz**; ZIF-412, -413, and -414, **ucb**; ZIF-516 and -586, **ykh**; ZIF-615, **gcc**; and ZIF-725, **bam**, respectively), and four of these **ykh**, **gcc**, **bam**, and **ucb** represent new topologies previously unknown in all porous crystals. According to common practice, zeolite topologies are given as capitalized, three-letter symbols, while new topologies are denoted by a three-letter symbol in bold, lowercase.[15−17]

Definition of Steric Index. The crystal structures of these new ZIFs showed a progression in the largest ring size, which is defined as

the number of Zn tetrahedral nodes in the ring and represents the pore opening. Eight-membered rings (8 MR) are present as the largest ring size in those ZIFs with CHA, LTA, KFI, and AFX topologies, while 12 MR in GME, **ucb**, and **moz**; 14 MR in **ykh**; 18 MR in **gcc**; and 24 MR in **bam** have been observed (Table 1).

Close examination of the ZIFs previously reported by us and others and earlier members (AFX and KFI) of the series we report here reveal a striking commonality: the 2- and 4,5-positions of Im linkers tend to point into the 4 MR and ≥8 MR, respectively. Both positions are usually found in the 6 MR because this is the ring sharing the 4 MR with ≥8 MR (Figure 1 and Figures S58−S72). We noted that the Im positions arrangement is generally followed; however, exceptions arise when the 4 MR is adjacent to another 4 MR through sharing of edges as for example in ZIFs of the MER topology, where the 2- and 4,5-positions have to point into a 4 MR.

The fact that the 4,5-position points into larger rings meant that ZIFs with much larger rings, and therefore larger pore openings, could be potentially achieved by introducing bulkiness in the Im linkers at that specific position. In principle, it might be possible to make large rings by adding a very bulky group to the 2-position; however, it is far more effective to introduce such bulkiness at the 4,5-position, and thus, this was the focus of our work. Indeed, we determined two relevant distances (l_2 and $l_{4,5}$) for Im (Figure 1) and considered the longer of these l for the linkers employed in our study. The steric index

Table 1. Chemical Compositions, Underlying Topologies, Maximum Ring Sizes (R_{max}), Aperture Size (d_a), Cage Size (d_c) of the Largest Cages, Specific Surface Area (A_{BET}), and Pore Size Distribution (PSD Max, Peak Maxima of the Largest Cage) for the Obtained ZIFs Compared with the State-of-the-Art ZIFs and Tetrahedral Inorganic Structures

material	composition	net	A_{BET} (m²/g)	R_{max} (MR)	d_a (Å)[a]	d_c (Å)[b]	PSD max (Å)[c]	ref
ZIF-303	$Zn(cbIM)_{0.70}(nIM)_{0.30}(IM)_{1.00}$	CHA	N/A	8	4.0	21.5	N/A	this work
ZIF-360	$Zn(bIM)_{1.00}(nIM)_{0.70}(IM)_{0.30}$	KFI	1050	8	4.8	27.8	11.0	this work
ZIF-365	$Zn(cbIM)_{0.95}(nIM)_{0.60}(IM)_{0.45}$	KFI	920	8	5.0	27.8	10.1	this work
ZIF-376	$Zn(nbIM)_{0.25}(mIM)_{0.25}(IM)_{1.50}$	LTA	N/A	8	6.9	27.5	N/A	this work
ZIF-386	$Zn(nbIM)_{0.85}(nIM)_{0.70}(IM)_{0.45}$	AFX	740	8	4.9	28.4 × 22.6	9.2	this work
ZIF-95	$Zn(cbIM)_2$	**poz**	1050	12	3.47	38.1 × 33.8	N/A	12
ZIF-100	$Zn_{20}(cbIM)_{39}(OH)$	**moz**	600	12	3.4	41.2	32.5	12
ZIF-408	$Zn(cbIM)_{1.86}(IM)_{0.09}(OH)_{0.05}$	**moz**	N/A	12	3.4	41.2	N/A	this work
ZIF-70	$Zn(nIM)_{0.87}(IM)_{1.13}$	GME	1730	12	13.2	22.6	N/A	18
ZIF-410	$Zn(cbIM)_{1.10}(aIM)_{0.90}$	GME	800[d]	12	5.2	22.6	8.9[d]	this work
ZIF-486	$Zn(nbIM)_{0.20}(mIM)_{0.65}(IM)_{1.15}$	GME	1180	12	6.0	22.6	9.9	this work
ZIF-412	$Zn(bIM)_{1.13}(nIM)_{0.62}(IM)_{0.25}$	**ucb**	1520	12	8.2	45.8	38.1	this work
ZIF-413	$Zn(mbIM)_{1.03}(nIM)_{0.64}(IM)_{0.33}$	**ucb**	1290	12	6.8	45.8	33.2	this work
ZIF-414	$Zn(nbIM)_{0.91}(mIM)_{0.62}(IM)_{0.47}$	**ucb**	1440	12	4.6	45.8	32.0	this work
ZIF-516	$Zn(mbIM)_{1.23}(bbIM)_{0.77}$	**ykh**	640	14	4.5	22.1	8.2	this work
ZIF-586	$Zn(mbIM)(2-mbIM)$	**ykh**	N/A	14	N/A	22.3	N/A	this work
ZIF-615	$Zn(cbIM)_{1.05}(4-nIM)_{0.95}$	**gcc**	770	18	14.5	27.2	11.4	this work
ZIF-725	$Zn(bbIM)_{1.35}(nIM)_{0.40}(IM)_{0.25}$	**bam**	720	24	22.5	39.0	31.1	this work
VPI-5	$Al_{18}P_{18}O_{72}$	VFI	N/A	18	12.0−13.0	16.3	N/A	24
ITQ-37	$Ge_{80}Si_{112}O_{400}H_{32}F_{20}$	ITV	690	30	4.3 × 19.3	25.0	10	25

[a]Aperture size (d_a) was estimated by fitting the largest sphere or ellipsoid into the largest ring with consideration of the van der Waals radius of all atoms. [b]Cage size (d_c) was estimated with the shortest Zn/Al/Si/P···Zn/Al/Si/P distance across the cage. [c]Pore size distribution (PSD) was assessed by the QSDFT/GCMC fitting using the corresponding N_2 physisorption isotherms at 77 K, only peak maximums were shown here (SI). The pore sizes derived from PSD maximums are smaller compared to the d_c due to the presence of Im linkers. [d]The values are obtained from activated sample, for which we note subtle changes in the PXRD peak position attributable to the slight rotation of the IM linkers along the axis between two Zn metals.

(δ) is defined as the product of the van der Waals volume (V) of Im and l, and it is a measure of the size and shape of the Im (Figure 1 and Table S16).

RESULTS AND DISCUSSION

Principle I: Steric Index versus Opening Sizes. Our new series of ZIFs and those previously reported are shown on a plot of the largest ring size versus the largest δ presented in a ZIF structure where a clear correlation is observed between these two parameters. Using this principle of high steric index enabled us to achieve ZIFs with the highest reported ring size [14 MR in ZIF-516 and 586 (**ykh**); 18 MR in ZIF-615 (**gcc**); and 24 MR in ZIF-725 (**bam**)], far exceeding the previous 12 MR record held by GME, CAN, AFI, **zea**, **poz**, and **moz** ZIFs; and the largest pore opening [14.5 Å in ZIF-615 (**gcc**), and 22.5 Å in ZIF-725 (**bam**)], far exceeding the previously record held by GME and AFI ZIFs (13.2 Å) (Figure 1 and Table 1).[10,12,14,18] We note that although the increment of linker bulkiness will influence the pore opening, however, we can clearly see that larger pore openings would be achieved in larger rings as illustrated here by **gcc** and **bam** ZIFs. We note that although large δ leads to large ring size (pore opening), it does not preclude the possibility of making smaller ring sizes when a combination of Im linkers are used, as discussed below. However, large rings are not obtained when Im linkers of small δ are used. The essence of the first principle is that the maximum value of δ leads to the *maximum* possible ring size and this determines the size of the pore opening.

Principle II: Linker Combinations versus Cage Sizes. Now we turn to ZIFs with large cages (large internal pores). It is apparent that large cages will not be easily achieved simply by increasing the value of δ alone (i.e., by employing bulkier Im).

This is because the formation of large cages requires both large rings but more critically a large number of small rings (i.e., 3 MR, 4 MR, and 6 MR) in tetrahedral structures,[19] and this latter condition is not always met by a large δ. For example, 6 MR is missing in all ZIFs constructed solely from cbIM or larger linkers (**poz**, **moz**, **zea**, and **ykh**). Thus, addition of nonbulky Im is equally important for making large cages, and intuitively, a balance must be struck when combining Im linkers of large and small δ. This is exemplified by comparison of ZIF-412 [$Zn(bIM)_{1.13}(nIM)_{0.62}(IM)_{0.25}$] with **ucb** topology and the already reported ZIF-68 [$Zn(bIM)(nIM)$] with GME topology. They both contain ZIF linkers of larger δ value (679 and 347 Å⁴ for bIM and nIM, respectively), which provide the 8 MR and 12 MR necessary to generate large cages. However, the addition of IM, which has a relatively smaller δ (248 Å⁴), leads to the formation of more small rings (4 and 6 MR) in the structure of ZIF-412, and therefore, this ZIF has a cage double the size of that found in ZIF-68 (Figure 2, Table 1, and Figures S63−S64).

It is clear from the discussion thus far that combining Im linkers with large and small δ and balancing their proportions are critical to achieving ZIFs with large cages. Figure 2 shows a plot of the correlation of the percentage of linkers with relatively large δ versus the resulting cage size in a ZIF. It reveals that progressively larger cages of diameter above 20 Å can be achieved if at least 25% of the bulky Im linkers (all Im linkers other than those with the smallest δ in the composition of a ZIF) are present. On the basis of this relationship, the three new **ucb** ZIFs (ZIF-412, -413, and -414) stand out as having the largest cage size among all ZIFs.
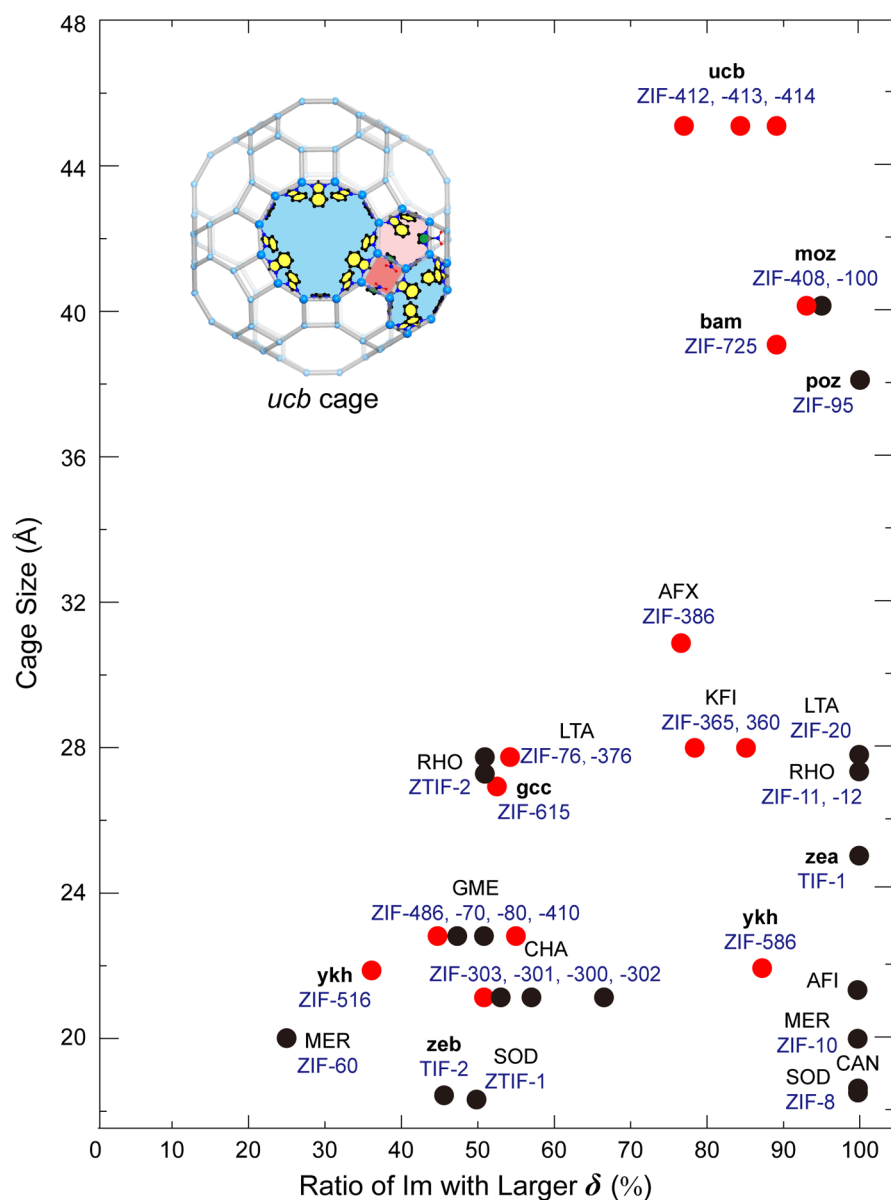
Figure 2. Distribution map of ideal cage sizes with the corresponding larger linker percentages in ZIF structures. The size of the largest cage in each topology is plotted versus the percentage of Im linkers with larger δ. Larger Im is indicated in ZIFs containing a combination of Im linkers, where it excludes the smallest Im in the set. ZIFs made solely from one Im linker are shown at 100%. ZIF structures with cage size less than 18 Å are not shown. Red dots represent structures reported here, and black dots represent those already reported. The inset, upper left, shows a schematic of the largest *ucb* cage in **ucb** ZIF-412. It reveals how the large rings (8 and 12 MRs) are joined through the smaller rings (4 and 6 MRs). The composition of these rings is also shown. Note that some imidazolates are aligned perpendicularly to the cage surface with their 2-positions pointing to the 4 MR perpendicular to the cage surface, which connects the cage into three-dimensional structures.

Previously, only eight topologies in ZIFs have shown large cage sizes: MER[1], 20.5 Å; CHA,[20] 21.5 Å; AFI,[14] 21.7 Å; GME,[10,17] 22.6 Å; **zea**,[18] 25.1 Å; RHO,[1,21] 27.3 Å; LTA,[9,10] 27.5 Å; **poz**,[12] 38.1 × 33.8 Å²; and **moz**,[12] 41.2 Å. Here, we report another six new topologies of large pore sizes: **ykh**, 22.3 Å; **gcc**, 27.2 Å; KFI, 27.8 Å; AFX, 28.4 × 22.6 Å²; **bam**, 39.0 Å; and **ucb**, 45.8 Å (cage size is estimated by the shortest Zn···Zn distance across the cage in order to compare the intrinsic difference of structure types, Figure 2 and Table 1).

Combining multiple Im linkers with smaller and larger δ values represents more fruitful work in achieving large cages compared to a single Im linker since we now can tune the small rings and larger rings, respectively, through the judicious selection of linker combinations. This is demonstrated for all

our new ZIF structures, most especially those with very large cages belonging to LTA, KFI, AFX, **gcc**, **bam**, and **ucb** topologies. Using this approach, we were also able to make a **moz** ZIF (ZIF-408) based on the combination of mIM and cbIM, further supporting our notion that multiple Im linkers facilitate the formation of ZIFs with large cages. We are cognizant that using too many Im linkers with small δ will compromise the formation of the largest cages. This is made clear by the appearance of ZIFs with the largest cages (**ucb** ZIFs) on the right side instead of the left side of the plot in Figure 2. The second principle emphasizes that since large cages require both small and large rings, using combinations of Im linkers of small and large δ greatly facilitates the formation of such cages.
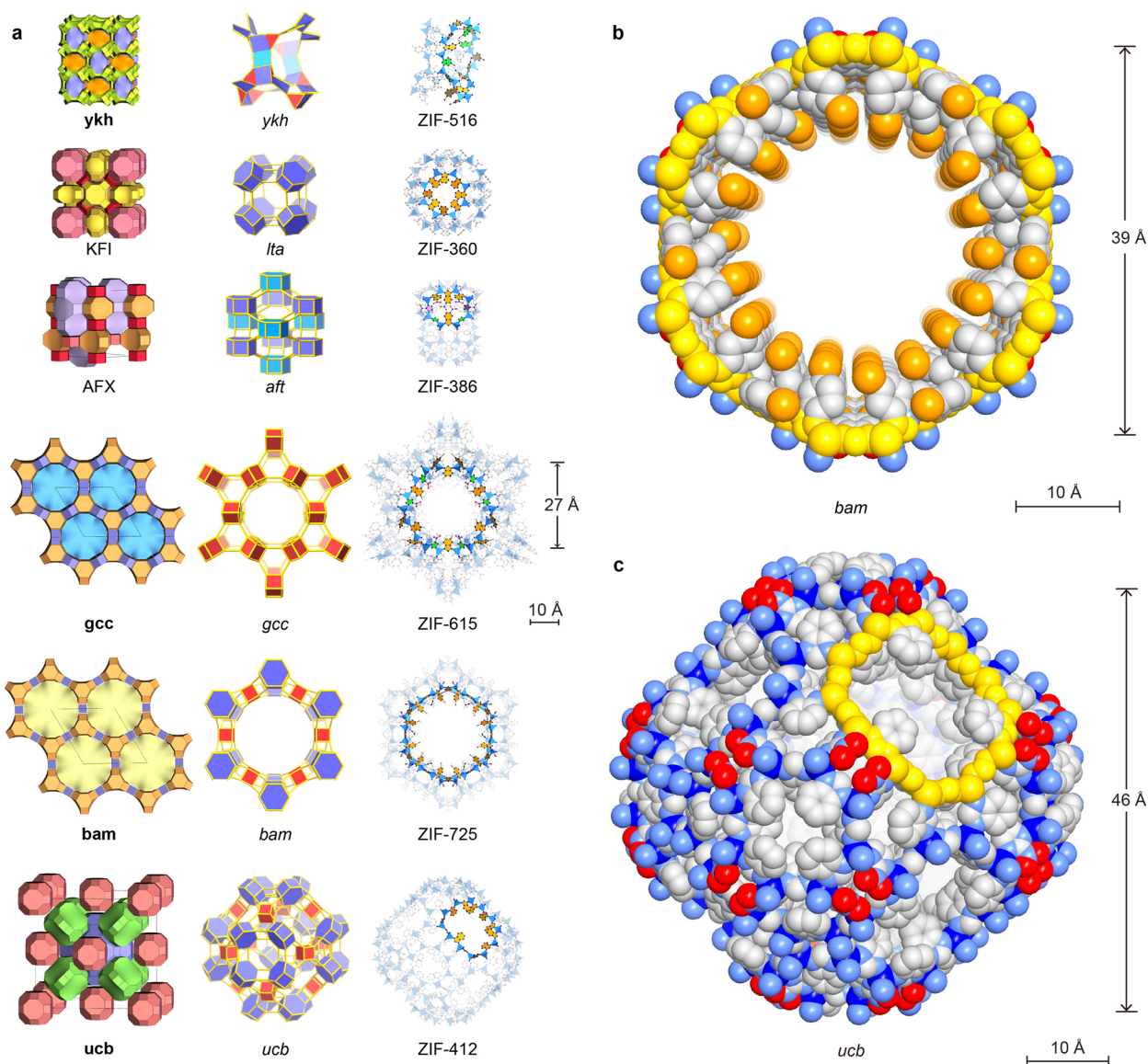
Figure 3. Crystal structures of the new ZIFs. Topologies are shown in natural tilings. The largest cages are presented with adjacent small cages, and characteristic cages are shown with ball-and-stick structures for linkers (N, blue; C, dark; O, red; Cl, green; Br, orange, H, omitted for clarity) and blue tetrahedra for ZnN_4 units. (a) KFI, ZIF-360; AFX, ZIF-386; **ykh**, ZIF-516; **gcc**, ZIF-615; **bam**, ZIF-725; **ucb**, ZIF-412. Largest openings for each cage are highlighted. (b) Space-filling views for the channel in **bam** ZIF (ZIF-725) are shown (zinc, blue; N, light blue; C, gray; O, red; Br, orange). The 24-MR aperture (**bam** ZIF-725, 96 atoms) is highlighted in yellow. (c) Space-filling view for the largest cage in **ucb** ZIFs (illustrated by ZIF-412) is shown: zinc, blue; N, light blue; C, gray; O, red. The 12 MR opening (**ucb** ZIF-412, 48 atoms) is highlighted in yellow.

Principle III: Linker Ratio versus Structure Tunability. The first and second principles provide clear guidelines for achieving pore metrics without putting limits on the number and functionality of the Im linkers. A general question arises: How can we create diversity from a given set of available linkers? On the basis of this study, we find that the ratio of Im linkers provides another handle for accessing ZIFs with a range of pore metrics. For example, the combination of IM (δ = 248 Å^4), mIM (δ = 319 Å^4), and nbIM (δ = 1064 Å^4), when employed in different ratios, gave us three new ZIFs that belong to three different topologies: ZIF-486 $[Zn(nbIM)_{0.20}$-$(mIM)_{0.65}(IM)_{1.15}$, GME], ZIF-376 $[Zn(nbIM)_{0.25}$-$(mIM)_{0.25}(IM)_{1.5}$, LTA], and ZIF-414 $[Zn(nbIM)_{0.91}$-$(mIM)_{0.62}(IM)_{0.47}$, **ucb**] with cage sizes of 22.6, 27.5, and 45.8 Å, respectively (Figure 2 and Table 1). In essence, the third principle points to an immense diversity to be exploited

for ZIF structures by varying the Im ratios, where not only are the maximum pore opening and cage size achieved but also any values up to the maximum. A point worth mentioning is that, as the number of Im types increases in ZIF, the power of this principle will be amplified in creating diverse structures and pore metrics.

Single Crystal Structure Illustration. The crystal structures of the 15 new ZIFs were determined by single crystal X-ray diffraction techniques, and those representing new topologies are shown in Figure 3 where the tilings, detailed cage topologies and crystal structures are shown (the largest ring highlighted). The cage name is denoted with a three-letter code in *italics* and lower-case, and the symbol $[...m^n...]$ means that the cage has n faces that are m-member rings.[22,23] For KFI and AFX ZIFs with 8 MR opening, the largest cages are *lta* $[4^{12}6^88^6]$ and *aft* $[4^{15}6^28^9]$, respectively; for **ykh** with a 14 MR opening, the
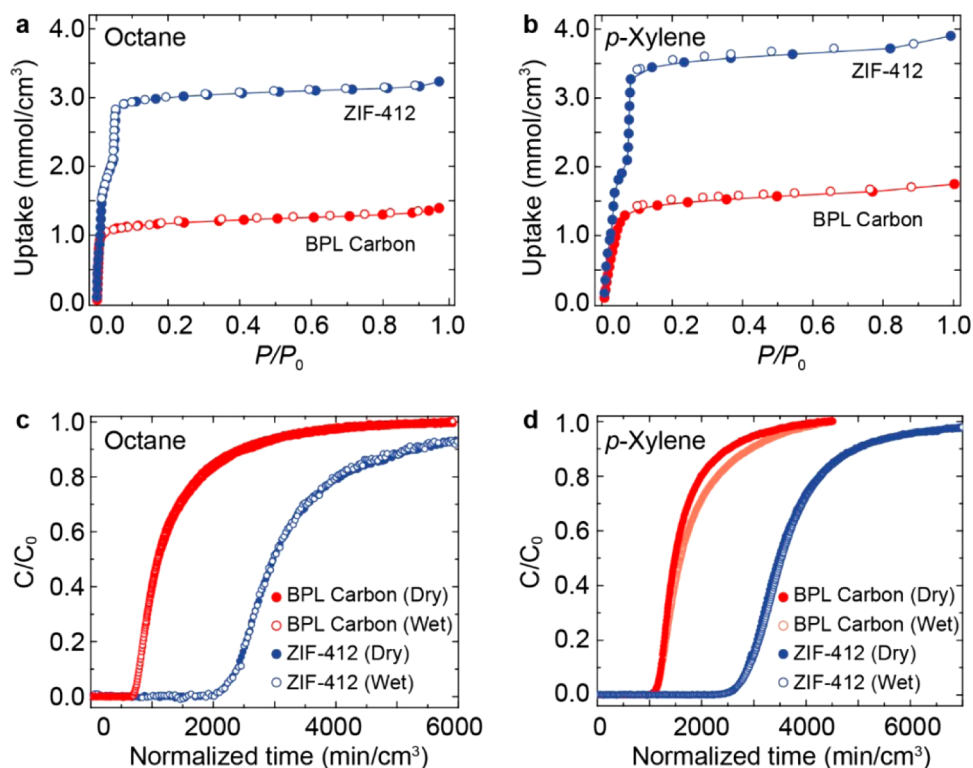
Figure 4. Octane and *p*-xylene removal using ZIF-412 and BPL carbon. (a) Static vapor adsorption isotherm at 298 K for octane (left), where ZIF-412 shows 260% more uptake than BPL carbon. (b) Static vapor adsorption isotherm for *p*-xylene (right), where ZIF-412 shows a 250% improvement in uptake. (c) Breakthrough curves under both dry and wet conditions (RH 0% and 65%, respectively) using ZIF-412 and BPL carbon at 298 K for octane. (d) Breakthrough curves for *p*-xylene. Solid circles represent breakthrough curves under dry conditions; empty circles represent breakthrough curves under wet conditions. ZIF-412 shows a much longer breakthrough time in comparison to BPL with and without the interference of water.

largest cage is *ykh* $[3^4 4^8 10^2 14^2]$ (Figure 3a). For **gcc** and **bam** ZIFs having one-dimensional cylindrical channels with 18 MR and 24 MR opening, respectively, the cages are *gcc* $[8^6 18^2]$ and *bam* $[4^6 8^6 24^2]$ (Figure 3a,b). The 24 MR opening in **bam** ZIF-725, composed of 96 ring atoms, has an aperture size of 22.5 Å in diameter, which is the largest among all tetrahedral structures (state-of-the-art GME ZIF-70 with an aperture size of 13.2 Å and zeolite VPI-5 of 12−13 Å)[17,24] (Table 1). We note that due to disorder of imidazolate, crystallographic aperture sizes of our ZIFs can only be estimated with full occupancy of the bulky imidazolates; thus, the real aperture sizes are underestimated and in fact are even larger. This is exemplified by the disorder of bulky bbIM and small IM in **bam** ZIF-725 as well as the disorder of bulky bIM and small IM in **ucb** ZIF-412 (Table 1).

The three **ucb** ZIFs, ZIF-412, -413, and -414, all crystallized in the high-symmetry cubic system (space group $Fm\bar{3}m$) with a unit cell length and volume exceeding 72 and 376000 Å^3, respectively, are among the largest unit cell volumes ever reported for synthetic crystals (Figure 3a,c).[12] These ZIFs have a hierarchical pore system with three type of cages: a truncated cuboctahedral *lta* $[4^{12} 6^8 8^6]$ with 8 MR opening; a tetrahedral *fau* $[4^{18} 6^4 12^4]$ with 12 MR opening; and a giant truncated octahedral *ucb* $[4^{36} 6^{24} 8^6 12^8]$ (shown in Figure 3a,c), which is composed of 144 vertices (ZnN$_4$) and 216 edges (Im) and a cage size of 45.8 Å in diameter, representing the largest porous cage ever made in all tetrahedral structures (state-of-the-art ZIF-100 with a cage size of 41.2 Å, and zeolite ITQ-37 with a cage size of 25 Å)[12,25] (Table 1). Recently, a discrete molecular cage compound with a larger size was reported (M$_{48}$L$_{96}$, 54.8 Å of the shortest Pd⋯Pd distance across the cage); however,

unlike the present ZIFs, investigation of its permanent porosity remains absent.[26]

Porosity Characterization. The pore size distribution derived from a N$_2$ gas adsorption study reveals a size of *ca.* 38.1 Å in diameter (peak maximum) of the *ucb* cages in ZIF-412 (Table 1), far exceeding the previous record held by ZIF-100 (with a size of *ca.* 32−33 Å) and zeolite ITQ-37 (*ca.* 10 Å). The gas N$_2$ adsorption isotherms at 77 K also gave Brunauer−Emmett−Teller (BET) surface areas in the range 640−1520 m^2/g for the majority of ZIFs (Table 1). The **ucb** and **bam** ZIFs exhibited type IV isotherms characteristic of mesopores, which is in agreement with their crystal structures. The **ucb** ZIFs reveal much higher BET surface areas (1290−1520 m^2/g), while the **bam** ZIF shows BET of 718 m^2/g, owing to the bulky bbIM linker.

VOC Removal Test from Humid Air. The remarkably large cage of ZIF-412, its permanent porosity, and hydrophobic interior led us to examine its performance in the removal of volatile organic compounds (VOCs), especially those of large molecular size. These commonly used molecules continue to be a major environmental and health concern because they are difficult to remove from sources where they are present in very low concentrations (ppm levels).[27−31] There are several requirements for a material to be employed for this purpose: (1) high capacity, (2) ability of uptake at low concentrations, (3) water stability and performance under wet conditions, and (4) cycling performance without losing capacity. Activated carbons have been extensively used; however, they suffer from relatively low capacity and difficulty in regeneration.[28] MOFs previously tested for this use show better uptake capacity in dry

conditions but not in the presence of water, a critical challenge and a prerequisite for this application.[32−34]

Here, we present the use of large pore ZIF-412 material to address these challenges. Its water adsorption isotherms show strong hydrophobicity (Figure S117). Static adsorption isotherms of octane and *p*-xylene, representatives of the aliphatic and aromatic VOCs, show that ZIF-412 can take up 3.0 mmol/cm^3 octane and 3.4 mmol/cm^3 *p*-xylene vapors at low partial pressure (P/P_0 = 0.1, 298 K), 2.6 and 2.5 times higher compared to that of BPL carbon, respectively (Figure 4a, b). These values are comparable to the best performing porous materials reported so far (3.2 mmol/cm^3 of octane in Mg-MOF-74 at P/P_0 = 0.08, 293 K; 3.7 mmol/cm^3 of *p*-xylene in Cr-MIL-101 at P/P_0 = 0.1, 298 K, both are under dry conditions).[33,34] Dynamic breakthrough experiments confirmed the VOC separation capability of ZIF-412: At a low concentration of octane (910 ppm) in a dry air stream, ZIF-412 showed a breakthrough time up to 2280 min/cm^3 (the time when outlet concentration reach 5% of the feed concentration), 3.0 times longer than BPL carbon under the same conditions (Figure 4c). This performance was unaltered for ZIF-412 under wet conditions (relative humidity, RH 65%, 298 K) and over three continuous cycles (Figure S121). In contrast, when BPL carbon was used, although the capacity remains the same in the presence of water, after the regeneration, in the subsequent second and third run, BPL carbon lost 28% of its original capacity indicated by the shortened breakthrough time after the first run (Figures S119 and S121). With respect to the best performing porous material tested so far, Mg-MOF-74, which has a high uptake of 3.2 mmol/cm^3 under dry conditions (293 K), its uptake diminished to 0.2 mmol/cm^3 in the presence of water (RH 80%, 293 K).[33] Similar to the results found for octane, the breakthrough tests for *p*-xylene (850 ppm) using ZIF-412 also show exceptional cycling performance in the presence of water. Specifically, the *p*-xylene breakthrough time for ZIF-412 is 2780 min/cm^3, with no loss of performance in the presence of water over three cycles (Figure 4d and Figure S122). We attribute the exceptional performance and stability of ZIF-412 material to its permanent porosity and hydrophobicity.

Finally, we remark that in this study we showed how, by using progressively bulkier linkers, it is possible to expand the pore openings and internal pores, rather than to constrict them as is typical in metal−organic framework chemistry.

■ ASSOCIATED CONTENT

ⓢ Supporting Information

The Supporting Information is available free of charge on the ACS Publications website at DOI: 10.1021/jacs.7b02272.

> Information on ynthesis, NMR, EA, IR, SCXRD, PXRD, TGA, gas adsorption, VOC adsorption and breakthrough, and Linker-ZIF structure correlation analysis (PDF)
> Crystal data for ZIF-303 (CIF)
> Crystal data for ZIF-360 (CIF)
> Crystal data for ZIF-365 (CIF)
> Crystal data for ZIF-376 (CIF)
> Crystal data for ZIF-386 (CIF)
> Crystal data for ZIF-408 (CIF)
> Crystal data for ZIF-410 (CIF)
> Crystal data for ZIF-412 (CIF)
> Crystal data for ZIF-413 (CIF)
> Crystal data for ZIF-414 (CIF)
> Crystal data for ZIF-486 (CIF)
> Crystal data for ZIF-516 (CIF)
> Crystal data for ZIF-586 (CIF)
> Crystal data for ZIF-615 (CIF)
> Crystal data for ZIF-725 (CIF)

■ AUTHOR INFORMATION

Corresponding Authors

*hdeng@whu.edu.cn
*yaghi@berkeley.edu

ORCID ⓘ

Jingjing Yang: 0000-0002-1192-7368
Yue-Biao Zhang: 0000-0002-8270-1067
Omar M. Yaghi: 0000-0002-5611-3325

Present Address

○School of Physical Science and Technology, ShanghaiTech University, Shanghai 201210, China.

Author Contributions

◆J.Y. and Y.-B.Z. contributed equally.

Notes

The authors declare no competing financial interest.

■ REFERENCES

(1) Park, K. S.; Ni, Z.; Côté, A. P.; Choi, J. Y.; Huang, R. D.; Uribe-Romo, F. J.; Chae, H. K.; O'Keeffe, M.; Yaghi, O. M. *Proc. Natl. Acad. Sci. U. S. A.* **2006**, *103*, 10186−10191.

(2) Phan, A.; Doonan, C. J.; Uribe-Romo, F. J.; Knobler, C. B.; O'Keeffe, M.; Yaghi, O. M. *Acc. Chem. Res.* **2010**, *43*, 58−67.

(3) Peng, Y.; Li, Y.; Ban, Y.; Jin, H.; Jiao, W.; Liu, X.; Yang, W. *Science* **2014**, *346*, 1356−1359.

(4) Zhang, J. P.; Zhang, Y. B.; Lin, J. B.; Chen, X. M. *Chem. Rev.* **2012**, *112*, 1001−1033.

(5) Eddaoudi, M.; Sava, D. F.; Eubank, J. F.; Adil, K.; Guillerm, V. *Chem. Soc. Rev.* **2015**, *44*, 228−249.

(6) Auerbach, S. M.; Carrado, K. A.; Dutta, P. K. *Handbook of Zeolite Science and Technology*; CRC Press: Boca Raton, FL, 2003.

(7) Tian, Y.-Q.; Chen, Z.-X.; Weng, L.-H.; Guo, H.-B.; Gao, S.; Zhao, D. Y. *Inorg. Chem.* **2004**, *43*, 4631−4635.

(8) Huang, X. C.; Lin, Y. Y.; Zhang, J. P.; Chen, X. M. *Angew. Chem., Int. Ed.* **2006**, *45*, 1557−1559.

(9) Hayashi, H.; Côté, A. P.; Furukawa, H.; O'Keeffe, M.; Yaghi, O. M. *Nat. Mater.* **2007**, *6*, 501−506.

(10) Banerjee, R.; Phan, A.; Wang, B.; Knobler, C.; Furukawa, H.; O'Keeffe, M.; Yaghi, O. M. *Science* **2008**, *319*, 939−943.

(11) Wu, T.; Bu, X.; Zhang, J.; Feng, P. *Chem. Mater.* **2008**, *20*, 7377−7382.

(12) Wang, B.; Côté, A. P.; Furukawa, H.; O'Keeffe, M.; Yaghi, O. M. *Nature* **2008**, *453*, 207−211.

(13) Zhang, J.; Wu, T.; Zhou, C.; Chen, S.; Feng, P.; Bu, X. *Angew. Chem., Int. Ed.* **2009**, *48*, 2542−2545.

(14) Shi, Q.; Xu, W.-J.; Huang, R.-K.; Zhang, W.-X.; Li, Y.; Wang, P.; Shi, F.-N.; Li, L.; Li, J.; Dong, J. *J. Am. Chem. Soc.* **2016**, *138*, 16232−16235 We note the reported pore opening is 15.6 Å without considering the van der Waals radius of the two H atoms (1.2 Å × 2), we deducted them and used value 13.2 Å for comparison (all other values are using the same standard).

(15) O'Keeffe, M.; Peskov, M. A.; Ramsden, S. J.; Yaghi, O. M. *Acc. Chem. Res.* **2008**, *41*, 1782−1789.

(16) Alexandrov, E. V.; Blatov, V. A.; Kochetkov, A. V.; Proserpio, D. M. *CrystEngComm* **2011**, *13*, 3947−3958.

(17) Banerjee, R.; Furukawa, H.; Britt, D.; Knobler, C.; O'Keeffe, M.; Yaghi, O. M. *J. Am. Chem. Soc.* **2009**, *131*, 3875−3877.

(18) Wu, T.; Bu, X.; Liu, R.; Lin, Z.; Zhang, J.; Feng, P. *Chem. - Eur. J.* **2008**, *14*, 7771−7773. We note that the 16 MR exists in the structure **zea** is inessential; it is the sum of essential rings. Only 3, 4, 10, and 12 MR are essential rings in **zea**, which determine the largest pore opening (12 MR) and tile $[4^2 12^4] + 2[3^4 4^2 12^2] + [3^8 4^{22} 10^4 12^4]$, as confirmed in *Reticular Chemistry Structure Resource*, http://rcsr.anu.edu.au/.

(19) Brunner, G. O. *Zeolites* **1990**, *10*, 612−614.

(20) Nguyen, N. T. T.; Furukawa, H.; Gándara, F.; Nguyen, H. T.; Cordova, K. E.; Yaghi, O. M. *Angew. Chem., Int. Ed.* **2014**, *53* (40), 10645−10648.

(21) He, C.-T.; Jiang, L.; Ye, Z.-M.; Krishna, R.; Zhong, Z.-S.; Liao, P.-Q.; Xu, J.; Ouyang, G.; Zhang, J. P.; Chen, X. M. *J. Am. Chem. Soc.* **2015**, *137*, 7217−7223.

(22) Blatov, V. A.; Delgado-Friedrichs, O.; O'Keeffe, M.; Proserpio, D. M. *Acta Crystallogr., Sect. A: Found. Crystallogr.* **2007**, *63*, 418−425.

(23) Anurova, N.; Blatov, V. A.; Ilyushin, G. D.; Proserpio, D. M. *J. Phys. Chem. C* **2010**, *114*, 10160−10170.

(24) Davis, M. E.; Saldarriaga, C.; Montes, C.; Garces, J.; Crowdert, C. *Nature* **1988**, *331*, 698−699.

(25) Sun, J.; Bonneau, C.; Cantín, Á.; Corma, A.; Díaz-Cabañas, M. J.; Moliner, M.; Zhang, D.; Li, M.; Zou, X. *Nature* **2009**, *458*, 1154−1157.

(26) Fujita, D.; Ueda, Y.; Sato, S.; Mizuno, N.; Kumasaka, T.; Fujita, M. *Nature* **2016**, *540*, 563−566.

(27) Khan, F. I.; Ghoshal, A. K. *J. Loss Prev. Process Ind.* **2000**, *13*, 527−545.

(28) Britt, D.; Tranchemontagne, D.; Yaghi, O. M. *Proc. Natl. Acad. Sci. U. S. A.* **2008**, *105*, 11623−11627.

(29) Vellingiri, K.; Szulejko, J. E.; Kumar, P.; Kwon, E. E.; Kim, K.-H.; Deep, A.; Boukhvalov, D. W.; Brown, R. J. C. *Sci. Rep.* **2016**, *6*, 27813.

(30) DeCoste, J. B.; Peterson, G. W. *Chem. Rev.* **2014**, *114*, 5695−5727.

(31) Barea, E.; Montoro, C.; Navarro, J. A. R. *Chem. Soc. Rev.* **2014**, *43*, 5419−5430.

(32) Glover, T. G.; Peterson, G. W.; Schindler, B. J.; Britt, D.; Yaghi, O. M. *Chem. Eng. Sci.* **2011**, *66*, 163−170.

(33) Zhao, Z.; Li, X.; Li, Z. *Chem. Eng. J.* **2011**, *173*, 150−157.

(34) Moghadam, P. Z.; Fairen-Jimenez, D.; Snurr, R. Q. *J. Mater. Chem. A* **2016**, *4*, 529−536.